Mon. Not. R. Astron. Soc. **000**, 000–000 (0000) Printed 20 June 2016 (MN LATEX style file v2.2)

The column density distribution of hard X-ray radio galaxies

arXiv:1606.05504v1 [astro-ph.HE] 17 Jun 2016

F. Panessa[1⋆], L. Bassani[2], R. Landi[2], A. Bazzano[1], D. Dallacasa[3,4], F. La Franca[5], A. Malizia[2], T. Venturi[4], P. Ubertini[1]

[1] *INAF - Istituto di Astrofisica e Planetologia Spaziali di Roma (IAPS-INAF), Via del Fosso del Cavaliere 100, 00133 Roma, Italy*
[2] *Istituto di Astrofisica Spaziale e Fisica Cosmica (IASF-INAF), Via P. Gobetti 101, 40129 Bologna, Italy*
[3] *Dipartimento di Fisica e Astronomia, Università di Bologna, via Ranzani, 1, 40127, Bologna, Italy*
[4] *Osservatorio di Radioastronomia (ORA-INAF), Via P. Gobetti 101, 40129 Bologna, Italy*
[5] *Dipartimento di Matematica e Fisica, Università degli Studi Roma Tre, via della Vasca Navale 84, 00146 Roma, Italy*

ABSTRACT

In order to investigate the role of absorption in AGN with jets, we have studied the column density distribution of a hard X-ray selected sample of radio galaxies, derived from the INTEGRAL/IBIS and *Swift*/BAT AGN catalogues ($\sim$ 7-10% of the total AGN population). The 64 radio galaxies have a typical FRII radio morphology and are characterized by high 20-100 keV luminosities (from 10^{42} to 10^{46} erg/s) and high Eddington ratios (Log L_{Bol}/L_{Edd} typically larger than ~ 0.01). The observed fraction of absorbed AGN ($N_H > 10^{22}$ cm^{-2}) is around 40% among the total sample, and $\sim$ 75% among type 2 AGN. The majority of obscured AGN are narrow line objects, while unobscured AGN are broad line objects, obeying to the zeroth-order predictions of unified models. A significant anti-correlation between the radio core dominance parameter and the X-ray column density is found. The observed fraction of Compton thick AGN is $\sim$ 2-3%, in comparison with the 5-7% found in radio-quiet hard X-ray selected AGN. We have estimated the absorption and Compton thick fractions in a hard X-ray sample containing both radio galaxies and non-radio galaxies and therefore affected by the same selection biases. No statistical significant difference was found in the absorption properties of radio galaxies and non radio galaxies sample. In particular, the Compton thick objects are likely missing in both samples and the fraction of obscured radio galaxies appears to decrease with luminosity as observed in hard X-ray non-radio galaxies.

Key words: galaxies: active — galaxies: Seyfert — radio continuum: galaxies — galaxies: jets

1 INTRODUCTION

Unification models for Active Galactic Nuclei (AGN) hypothesize a common structure for the central engine, where the different orientation of the line-of-sight determines a different classification of the source (Antonucci 1993, Urry & Padovani 1995). Material accretes around a central super massive black hole in the form of a disk, often surrounded by a corona of hot electrons responsible of the emission at high X-ray energies. At larger scales, a dusty torus obscures the inner region of the AGN, reducing the amount of observable X-ray radiation. Moreover, the torus obscures the optical broad emission lines produced in the broad line region located within parsec scales from the nucleus, but it does not obscure the optical narrow emission lines produced at kpc scales from the nucleus. According to this picture, type 1 AGN show broad and narrow lines in their optical spectra as they are viewed face-on, while type 2 AGN only display narrow emission lines as they are viewed edge-on. This picture is confirmed by the presence of large amount of obscuration in the X-ray spectra of type 2 AGN and the little absorption in type 1 (e.g., Risaliti et al. 1999, Bassani et al. 1999).

The fraction of obscured AGN is important for the understanding of the nature of the circumn-nuclear medium, but it is also fundamental to characterize the history of black hole accretion in the Universe (Alexander et al. 2005, Gilli

⋆ E-mail: francesca.panessa@iaps.inaf.it

et al. 2007). Multi-wavelength surveys have attempted to constrain the number of obscured ($N_H > 10^{22}$ cm^{-2}) and Compton thick AGN (CT, $N_H > 10^{24}$ cm^{-2}), in the optical (e.g., Risaliti et al. 1999, Cappi et al. 2006, Panessa et al. 2006, Akylas & Georgantopoulos 2009, Jia et al. 2013, Vignali et al. 2014), infrared (e.g., Fiore et al. 2009, Alexander et al. 2011, Brightman & Nandra 2011) and hard X-rays (e.g., Sazonov et al. 2008, Malizia et al. 2009, Burlon et al. 2011). Hard X-rays surveys should be able to detect obscured AGN with less biases, however, even at energies > 10 keV, part of the intrinsic flux is reduced by obscuration to a level below the survey detection limit of current missions, leading to an observed fraction of CT AGN of a few percent (e.g., Ajello et al. 2008, Malizia et al. 2009, 2012, Burlon et al. 2011, Vasudevan et al. 2013), when correcting for biases this fraction rises to around 20-30%.

The fraction of obscured AGN appear to decrease with increasing observed X-ray luminosity in the local and distant Universe (e.g., Ueda et al. 2003, La Franca et al. 2005, Sazonov et al. 2007, Burlon et al. 2011, Ueda et al. 2014, Aird et al. 2015, Buchner et al. 2015), this effect is likely due to the decrease of the covering factor of the obscuring material with the luminosity, however this result has been questioned by Sazonov et al. (2015). A similar dependency has been found also with redshift (the fraction of absorbed objects increases toward higher redshifts), although this result is more controversial (e.g., La Franca et al. 2005, Treister & Urry 2006, Ueda et al. 2014); even at $z > 2$ larger absorption fractions are found in high luminosity AGN (Iwasawa et al. 2012).

In this work we investigate the role of absorption in radio galaxies. Does the presence of a jet influence the level of obscuration in AGN? Radio galaxies launch relativistic jets on large scales (from sub-kpc to Mpc) and are strong emitters in the radio band. Fanaroff & Riley (1974) classified radio galaxies into two classes, based on their radio power and morphology: the low luminosity radio galaxies (FRI) usually show a core, and twin jets (on average symmetric in brightness) which lose collimation at some distance from the core to form radio lobes; in the high luminosity sources (FRII) the radio jets are faint, or invisible, and culminate in high surface brightness regions (hot spots), with the radio lobes being backflow emission. This morphological classification is not sharp, and intermediate and/or hybrid morphologies can be found (Capetti, Fanti & Parma, 1995).

Radio galaxies have been also classified in low-excitation radio galaxies (LERGs) and high-excitation radio galaxies (HERGs) based on the optical emission lines from the nuclei (see Hine & Longair 1979). Most FRI and a subset of low radio power FRII are LERGs and also a few HERGs show an FRI morphology. It is believed that LERGs are inefficiently accreting objects and that their radio through X-ray nuclear emission is produced within their small-scale jet, while the emission in HERGs is likely accretion dominated (Chiaberge, Capetti & Celotti 2002, Hardcastle, Evans & Croston 2006). Moreover, HERGs show evidence for strong cosmic evolution at all radio luminosities, indicating a tendency of being located at larger distances, while LERGs are consistent with little or no evolution. A possible scenario is that HERGs might be fueled at relatively high rates in radiatively efficient standard accretion discs by cold gas, perhaps brought in through mergers and interactions, and with some of the cold gas leading to associated star-formation (Best & Heckman 2012). So far, no clear dividing factor between the FRI and FRII sources is found even when combining radio luminosity, accretion mode, large-scale environment and host galaxy luminosity (Gendre et al. 2013).

Early X-ray studies of radio galaxies revealed a large fraction of obscured nuclei, with narrow line radio galaxies showing column densities between 10^{21} and 10^{24} cm^{-2}, in agreement with the unification predictions (Sambruna et al. 1999). An anti-correlation between the absorbing column density and the radio core dominance parameter is found, suggesting that the absorption increases as the jet orientation angle decreases, in agreement with the unified models (Grandi et al. 2006, Wilkes et al. 2013). Most of the X-ray studies on radio galaxies are based on individual sources and only few works are performed on statistically significant samples. One example is the X-ray study of 22 radio galaxies which shows that FRI typically have much lower intrinsic absorption than FRII (Evans et al. 2006). Similarly, LERGs are generally X-ray weak with little or no absorption (Hardcastle et al. 2006), suggesting that the torus itself is missing or receeding as a consequence of the inefficient accretion regime (Lawrence 1991). A large fraction of obscured AGN is also found in a larger sample of ~ 40 narrow line radio galaxies (Hardcastle et al. 2009), but no CT radio galaxy is found. Recently, a study of 38 high redshift ($1< z < 2$) low frequency selected (178 MHz) 3CRR radio galaxies recovers a CT fraction of $\sim 20\%$ (Wilkes et al. 2013), found by means of multi frequency diagnostics to unveil CT candidates otherwise missed by simple hardness ratio arguments. However, in the local Universe, only a handful of CT radio galaxies are found (e.g., Hardcastle, Evans & Croston 2006, Eguchi et al. 2009, Guainazzi et al. 2006, Guainazzi et al. 2004). This very low fraction of CT radio galaxies is puzzling and whether it is due to evolution or selection effect must be clarified.

Since 2002, INTEGRAL/IBIS and later on *Swift*/BAT are surveying the sky at energies greater than 10 keV, releasing all sky catalogues that contain a large number of AGN, some previously known and others discovered for the first time at hard X-rays (Bird et al. 2010; Krivonos et al. 2010; Cusumano et al. 2010; Baumgartner et al. 2013). The hard X-ray selection is sensitive to gas rather than dust obscuration and should therefore allow the detection of highly obscured AGN, mostly mildly CT AGN with column densities in the range between 10^{24} - 10^{25} cm^{-2} where the continuum radiation should be visible above 10 keV.

In this work we present for the first time the column density distribution of a sample of radio galaxies selected at hard X-rays from INTEGRAL and *Swift* observations. The paper is organized as follows: in section 2 we present the radio galaxy sample and the X-ray data; in section 3 we report on the column density distribution and comment on some peculiar objects; in section 4 we discuss the fraction of obscured and CT AGN and in section 5 we present our conclusions. Throughout this paper we assume a flat ΛCDM cosmology with $(\Omega_M, \Omega_\Lambda) = (0.3,0.7)$ and a Hubble constant of 70 km s^{-1} Mpc^{-1} (Jarosik et al. 2011).

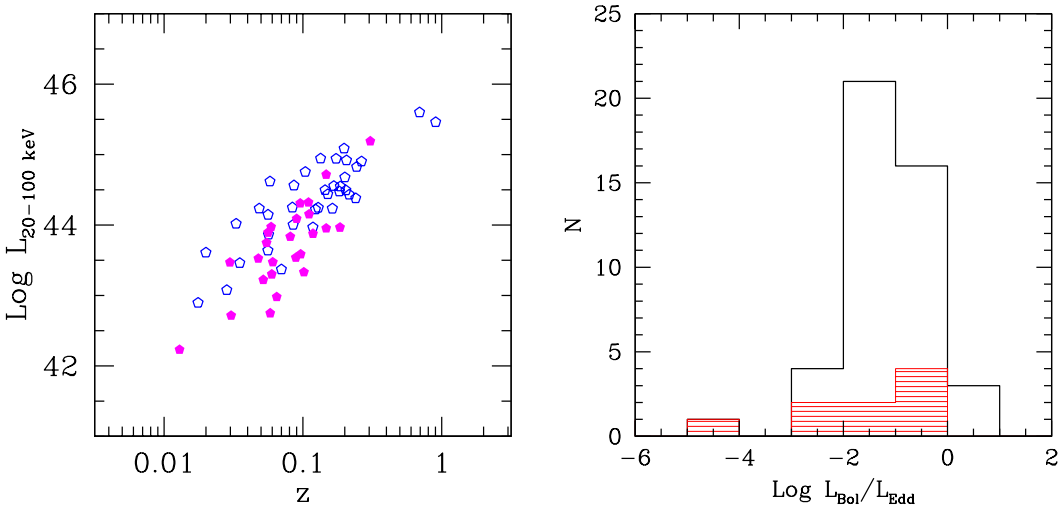

Figure 1. Bilogarithmic plot of the 20-100 keV luminosity versus redshift (left panel), blue empty points are type 1 AGN, while magenta filled points are type 2 AGN. In the right panel, the distribution of the ratio between the bolometric luminosity and the Eddington luminosity for the total sample, where red shaded histogram represents FRI and intermediate FRI/FRII radio galaxies.

2 THE SAMPLE AND THE X-RAY DATA

For the purpose of this work we have used the same sample of radio galaxies as in Bassani et al. (2016, accepted), except for three candidate sources for which the radio galaxy classification is uncertain and that we have not considered in this work. In Bassani et al. (2016), AGN from hard X-ray catalogues have been selected looking for extended radio emission. The hard X-rays catalogues considered are: (1) the sample of 272 INTEGRAL AGN discussed by Malizia et al. (2012), with a few additional sources discovered or identified as AGN afterwards (Landi et al. 2010, Masetti et al. 2013, Krivonos et al. 2012), and (2) the 70 months *Swift*/BAT AGN catalogue of Baumgartner et al. (2013) which lists 822 objects associated with AGN or galaxies; a sample of 65 objects classified as 'unknown' has also been included in an attempt to uncover all possible radio galaxies in the BAT sample. In Bassani et al. (2016), the NRAO VLA Sky Survey (NVSS, Condon et al. 1998) and the Sydney University Molonglo Sky Survey (SUMSS, Mauch et al. 2003) were used to assess the morphology and derive the radio power of the hard X-ray selected AGN. The morphological classification of our sample follows Fanaroff & Riley (1974), and is based on the radio morphology (core, jets, lobes and hotspots) and radio power; the transition power between FRI and FRII being roughly set at log P(1.4 GHz) = 24.5 W/Hz (Owen & Laing 1989).

The final sample is made of 64 hard X-ray selected radio galaxies, 22 from Malizia et al. (2012) plus four additional INTEGRAL sources lately identified as radio galaxies[1]: 22 AGN are of type 1, 19 of type 2 and 21 of intermediate class. The intermediate AGN are themselves split in 12 objects of early type (1.2-1-5) and 9 of late type (1.8-19) Seyfert classification. One source in the sample, IGR J13107-5626, has no redshift nor an optical classification, while PKS1737-60 has a photometric redshift and no optical classification. The majority of the sample has a radio morphological classification as FRII, with only six FRI and six intermediate FRI/FRII. FRII are likely associated to high excitation radio galaxies (Buttiglione et al. 2009) accreting at high Eddington ratios, in this sense, their dominance is expected in a hard X-ray selected sample.

The X-ray fluxes and column densities are taken from the literature (see column 9 in Table 1 for references) except for 16 objects for which we have analyzed XRT+BAT broad band spectra (see Appendix A for details on the X-ray analysis). In Figure 1 we plot the 20-100 keV X-ray luminosity versus redshift (left panel). It is clear that hard X-rays selects nearby very luminous radio galaxies, with 20-100 keV luminosities ranging from 10^{42} to 10^{46} erg/s. Black hole masses have been collected from the literature (column 11 for references), ranging from $\sim 10^7$ to 10^9 $M_\odot$[2]. In Figure 1 (right panel) we plot the distribution of the ratio between the bolometric luminosity and the Eddington luminosity (the bolometric luminosity is derived by applying a correction factor of 20 to the 2-10 keV luminosity, see Vasudevan & Fabian 2007). The Eddington ratios are relatively high suggesting that the hard X-ray radio galaxies are efficiently accreting sources and that their X-ray emission is likely dominated by the disk-corona system even in those galaxies with the most powerful jets (e.g., Reynolds et al.

[1] IGR J13107-5626 from Bassani et al. (2016), IGR J14488-4008 from Molina et al. (2015), IGR J17488-2338 from Molina et al. (2014) and 4C+21.55 from Bassani et al. (2016). and 60 from the *Swift*/BAT AGN catalogue. Twenty-two sources have been detected both by INTEGRAL and *Swift*/BAT. Radio galaxies represent $\sim$ 7-10% of the total AGN population at hard X-rays. The sample is presented in Table 1. In column three we report the optical classification of the sample (see Bassani et al. 2016)

[2] Different methods have been used in literature to estimate the black hole mass, therefore the values reported are not homogeneously derived, introducing a source of uncertainty which is difficult to estimate.

2015). The only source accreting at a low Eddington rate is Cen A, for this source it has been proposed that the hard X-ray emission is dominated by an Advection Dominated Accretion Flow (e.g., Fuerst et al. 2015) and its detection is likely due to its closeness.

3 THE COLUMN DENSITY DISTRIBUTION

The column density distribution of radio galaxies has been studied in samples selected either in the X-rays (Sambruna et al. 1999) or in the radio (Evans et al. 2006, Hardcastle et al. 2009, Wilkes et al. 2013). Narrow line radio galaxies typically show large X-ray column densities in agreement with the unified models, however the number of CT AGN has always been very small, quite below the 20-50 % fraction observed in local non-radio galaxies samples. In the left panel of Figure 2 we report the column density distribution of type 1 (black histogram) and type 2 AGN (blue shaded histogram). Intermediate Seyfert galaxies of early type classification (1.2-1.5) have been included in the type 1 group, while the late type (1.8-1.9) intermediates are included in the type 2 group. As expected, type 2 radio galaxies are typically more absorbed than type 1, with the distribution peaking in the range between 10^{23} cm^{-2} and 10^{24} cm^{-2}. In particular sources with $N_H > 10^{22}$ cm^{-2} are 26/64 ($\sim 40^{+13}_{-11}$ %) among the total sample and 21/28 (75^{+13}_{-9} %) among type 2 Seyferts in agreement with the observed fractions found in optically selected samples of non-radio galaxies. On the other hand only one source is CT (NGC 612) while VII Zw 292 has a column density consistent with the CT limit within an error of 90%, implying that the observed fraction of CT AGN is around 2-3% (< 11%) among the total sample and 4-7% (< 23%) among type 2 sources[3].

When low quality X-ray spectra do not allow a proper estimate of the real column density, it is possible to miss some CT AGN in a given sample. A diagram proposed by Malizia et al. (2007) uses the N_H versus softness ratio ($F_{2-10keV}/F_{20-100keV}$) to unveil hidden CT AGN, its validity has been proven by several other works (Ueda et al. 2007, Winter et al. 2008, Matt et al. 2012). Misclassified CT objects populate the part of the diagram with low absorption and low softness ratios, as the 2-10 keV flux is suppressed by absorption, while the 20-100 keV is less affected by absorption. The N_H versus the ratio between the observed 2-10 keV and 20-100 keV of the radio galaxy sample is plotted in Figure 2 (right panel): no source populates the bottom left part of the diagram suggesting that there are no hidden mildly CT AGN in the sample.

3.1 X-ray absorption versus optical and radio classification

Similarly to what found in non-radio galaxies hard X-ray samples, a small fraction of objects are 'outliers', i.e., exceptions to the unified models such as type 1 AGN with absorption and type 2 AGN without absorption (see Malizia et al. 2012). Six objects with broad emission lines (type 1, type 1.2 and type 1.5) display column densities $> 10^{22}$ cm^{-2}. IGR J17488–2338 and 4C50.55 are absorbed by one (Malizia et al. 2014) and two (Molina et al. 2007) layers of cold material partially covering the central source, respectively. Similarly in 3C 227 and PKS 2135-14 intrinsic absorption has been measured from the Chandra spectrum (Mingo et al. 2014). The XMM-Newton spectrum of IGR J14488-4008 is characterized by absorption due to ionized elements (Molina et al. 2015) and the presence of a warm absorber component is also found in 3C445 (Torresi et al. 2012). It is therefore likely that in most of these type 1 AGN ionized material located just off the torus and/or accretion disc might be responsible for the X-ray absorption.

Type 2 objects without X-ray absorption are another type of 'outliers' with respect to the unified models, where a column density $< 10^{21}$ cm^{-2} is not enough to obscure the BLR and the lack of broad emission lines in the optical spectrum is likely due to an absent or very weak broad line region (Panessa & Bassani 2002, Bianchi et al. 2012). In this sample, only PKS 2331–240 is a type 2 radio galaxy without absorption and it is the subject of a recent multi-wavelength observational campaign conducted by our team, which will be presented in a forthcoming publication.

Osterbrock (1981) introduced the notations Seyfert 1.5, 1.8 and 1.9, where the subclasses are based on the optical appearance of the spectrum, with the numerically larger subclasses having weaker broad-line components relative to the narrow line ones. According to unified models, at these intermediate classifications should correspond an intermediate inclination of the line of sight with respect to the obscuring torus, therefore type 1.8-1.9 should be mildly absorbed at X-rays (Risaliti et al. 1999). In our sample three sources are classified as type 1.8 Seyferts (3C 059, B3 0749+460A and PKS 1916-300) and show absorption consistent with the Galactic one, suggesting that the broad line components maybe intrinsically weak. However, Trippe et al. (2010) have shown that a large fraction of 1.8 and 1.9 were misclassified due to an overestimation of the flux of broad H_α, while others received this designation because of their low continuum flux. Accurate observations at multi epochs are therefore necessary to explore these possibilities.

In previous surveys, FRI radio galaxies have usually shown less absorption than FRII. In this sample, FRI and intermediate FIR/FRII, though numerically inferior, display a column density distribution similar to that of FRII. Interestingly, two out of five of the FRI in the sample are heavily absorbed (Cen A and PKS 2014-55). Three out of six intermediate FRI/FRII show $N_H > 5 \times 10^{22}$ cm^{-2}, i.e., 4C+29.30, 3C433 and NGC 612.

3.2 The radio core dominance versus absorption

The radio core dominance is defined as $R_{core} = S_{core}/(S_{tot} - S_{core})$, where S_{core} and S_{tot} are the core and the total flux densities at 5 GHz, respectively. It has been used as an orientation indicator, as objects with a large R_{core} should emit their radiation in a direction closer to the line of sight. Indeed, a strong anti-correlation between the X-ray column density and R_{core} has been found in samples of radio galaxies (e.g., Grandi et al. 2006, Wilkes et al. 2013). A significant anti-correlation between R_{core} and the inclination of

[3] Throughout the paper the standard error on the sample proportions in the binomial standard deviation for small samples are calculated at 2 σ (Gehrels 1986).

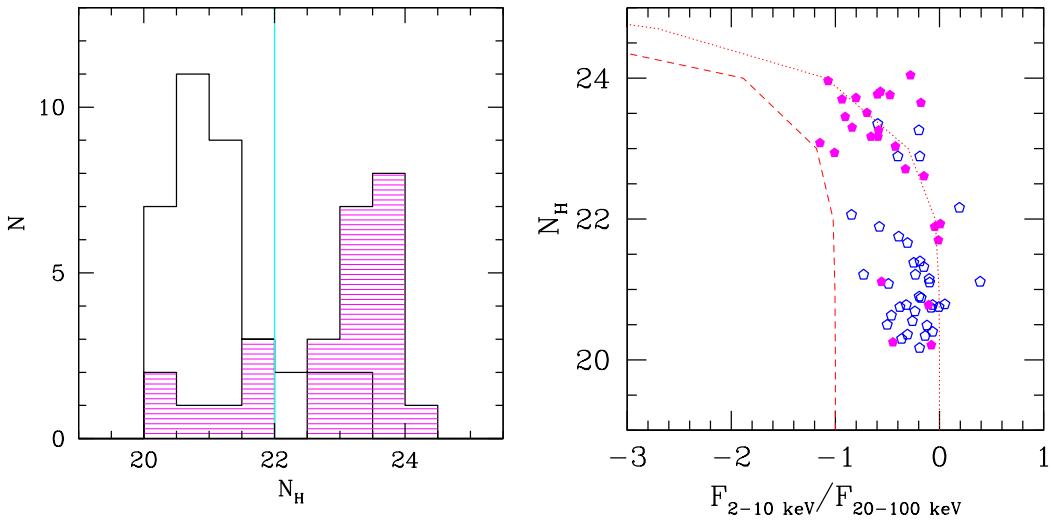

Figure 2. Column density distribution in cm^{-2}, type 1 are represented by the black histogram while type 2 by the magenta shaded histogram (left panel). A cyan line divides obscured objects ($N_H > 10^{22}$ cm^{-2}) from unobscured objects. Column density distribution in cm^{-2} versus the $F_{2-10keV}/F_{20-100keV}$ (right panel). Blue empty points are type 1 AGN, while magenta filled points are type 2 AGN. Lines correspond to expected values for an absorbed power law with photon indices 1.5 (dot) and 1.9 (dash) as in Malizia et al. (2012).

the dusty torus (derived from modeling the infrared spectral energy distribution) has also been found (Drouart et al. 2012). We have collected the R_{core} values at 5 GHz [4]. We have correlated the X-ray column density with R_{core} (see Figure 3). The Spearman's Rho correlation coefficient is -0.50 with a two-tailed value of the null hypothesis probability of correlation of 0.00027, suggesting that also among our sample of radio galaxies the two quantities are anti-correlated, in agreement with unified models. No correlation is found between R_{core} and the 2-10 keV luminosity nor the 20-100 keV luminosity. Note, however, that the calculation of R_{core} parameter relies on data taken at different epochs, with different instruments and at different linear scales. An appropriate set of radio images at the same frequency and with about the same linear resolution is fundamental in this respect for a proper determination of the radio core dominance parameter.

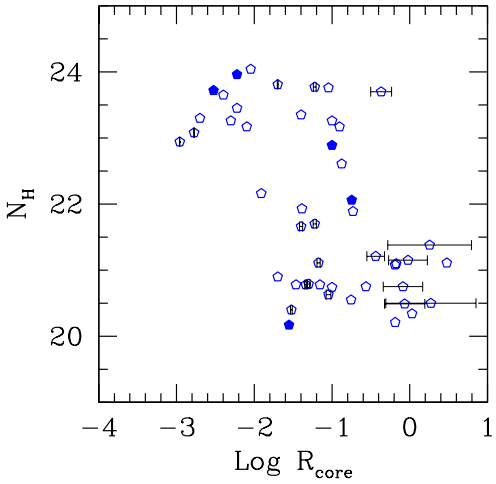

Figure 3. Column density versus the radio core dominance parameter R_{core} estimated at 5 GHz. Filled points have a R_{core} estimated at 1.4 GHz.

4 THE FRACTION OF ABSORBED AND COMPTON THICK RADIO GALAXIES

The determination of an intrinsic column density distribution, not affected by biases, is a hard task, even for the current hard X-ray surveys, where above 10-15 keV a significant fraction (up to 50-60%) is missed for $N_H > 3 \times 10^{24}$ cm^{-2} (Malizia et al. 2009, Ajello et al. 2009). Therefore the absorption bias limits the detection of Compton-thick objects only to those with bright fluxes and in the very local Universe. Malizia et al. (2009) recover a fraction of 20-30% of CT by limiting the sample to z<0.015, similarly Burlon et al. (2011) have found a fraction of 20% CT AGN by correcting for the absorption bias in the *Swift*/BAT sample. In order to evaluate the distance and flux biases among hard X-ray selected radio galaxies, we have estimated the fraction of absorbed and CT AGN in a sample containing both non-radio galaxies and radio galaxies selected at hard X-rays and therefore, subject to the same biases effects. We have considered the total INTEGRAL AGN sample in Malizia et al. (2012) in which 22 out of 271 AGN are radio galaxies. In Figure 4 we present the column density distribution of non-radio galaxies (black histogram) and radio galaxies (green shaded histogram). The fraction of absorbed AGN is 49^{+6}_{-7}% (121/249) among non-radio galaxies compared to 36^{+21}_{-16}% (8/22) among radio galaxies, while the fraction of CT AGN

[4] For five objects data were available at 1.4 GHz, while R_{core} in Fan & Zhang (2003) were calculated using extended luminosities at 1.4 GHz, assuming two possible values of the spectral index (α = 0.5 and α = 1.0) to convert the 1.4 GHz luminosity into 5 GHz luminosity (see their work for details).

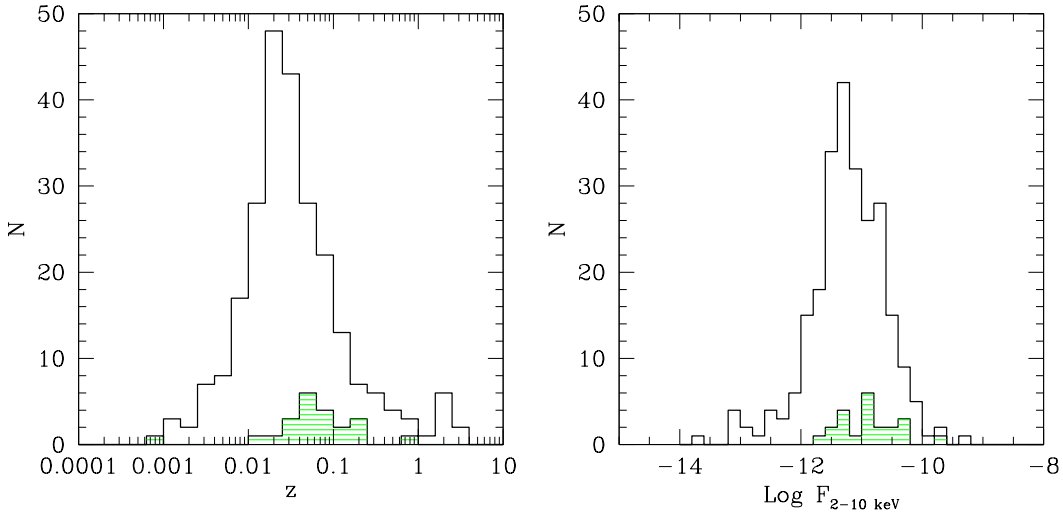

Figure 5. Left panel: redshift distribution of non-radio galaxies and radio galaxies (shaded green) of the Malizia et al. (2012) INTEGRAL sample. Right panel: 2-10 keV flux distribution of non-radio galaxies and radio galaxies (shaded green) of the Malizia et al. (2012) INTEGRAL sample.

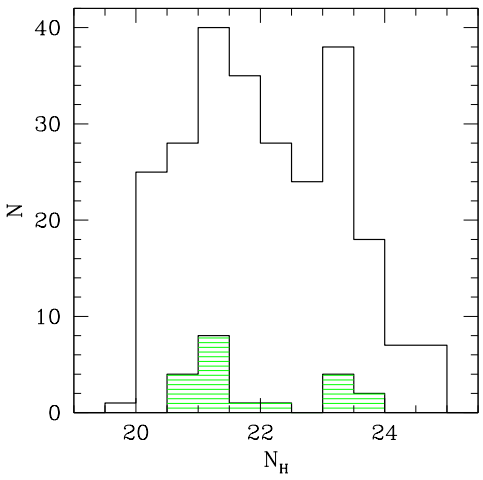

Figure 4. Column density distribution of non-radio galaxies (black histogram) and radio galaxies (shaded green) of Malizia et al. (2012).

is 6±3% (14/249) compared to 0/22 (<1. 3%) among radio galaxies.

In Figure 5 (right panel), we have compared the redshift distribution of non-radio galaxies and radio galaxies (in green) separately. We have tested the null hypothesis that the two samples are taken from populations with the same redshift distribution using the Kolmogorov–Smirnov (K-S) test at a significance level of $\alpha = 0.01$. The derived p-value is 0.0014, therefore the null hypothesis can be rejected at 1% level. It is remarkable that no radio galaxies are found below z<0.01 (except for the peculiar source Cen A) in agreement with the fact that HERGs are preferentially found at larger distances than LERGs.

Excluding Cen A, we have selected all non-radio galaxies in Malizia et al. (2012) in the redshift regime where all radio galaxies are found, i.e. z>0.01. We have then compared the column density distribution of the two selected sub-samples. At these redshifts, the observed fraction of absorbed AGN among non-radio galaxies is 42^{+7}_{-6}% (89/212) consistent with the observed fraction in radio galaxies of 33^{+22}_{-16}% (7/21), similarly the fraction of CT sources among non-radio galaxies is 9/212 (4^{+4}_{-2}%) compared with that of radio galaxies (0/21, <1. 4%). In Figure 5 (left panel), the 2-10 keV flux distribution of non-radio galaxies and radio galaxies (in green) is shown. In this case, the derived KS p-value is 0.047, therefore the null hypothesis that the two samples are taken from populations with the same flux distribution cannot be rejected at 1% level. No radio galaxies are found below $\sim 10^{-12}$ ergs cm^{-2} s^{-1}, therefore we have selected all non-radio galaxies with $F_{2-10keV} > 10^{-12}$ ergs cm^{-2} s^{-1}. In this case the fraction of CT objects among non-radio galaxies (14/227, 6^{+4}_{-2}%) is only slightly larger than that of radio galaxies, 0/22 (<1. 3%), while the fraction of absorbed AGN in non-radio galaxies (107/227, 47^{+7}_{-6}%) is again consistent within errors with that of radio galaxies (8/22, 36^{+21}_{-16}%). The above results suggest that radio galaxies might be affected by the same redshift bias as non-radio galaxies, suggesting that we are probably missing CT AGN in both classes of objects. However, the marginal evidence of a lower fraction of CT AGN in radio galaxies deserves deeper investigation through larger samples of objects.

We have explored a possible dependence of the observed fraction of absorbed AGN with luminosity. In Figure 6 we show the dependence of the absorbed fraction in our sample of 64 radio galaxies with the intrinsic hard X-ray luminosity (left panel). Sources have been grouped in order to have nearly the same number of objects in each bin. We find a trend of decreasing obscured sources with luminosity, in agreement with the results from X-ray surveys. We have done the same exercise on the sample by Malizia et al. (2012), separating radio galaxies from non-radio galaxies (right panel). Unfortunately the number of radio galaxies is

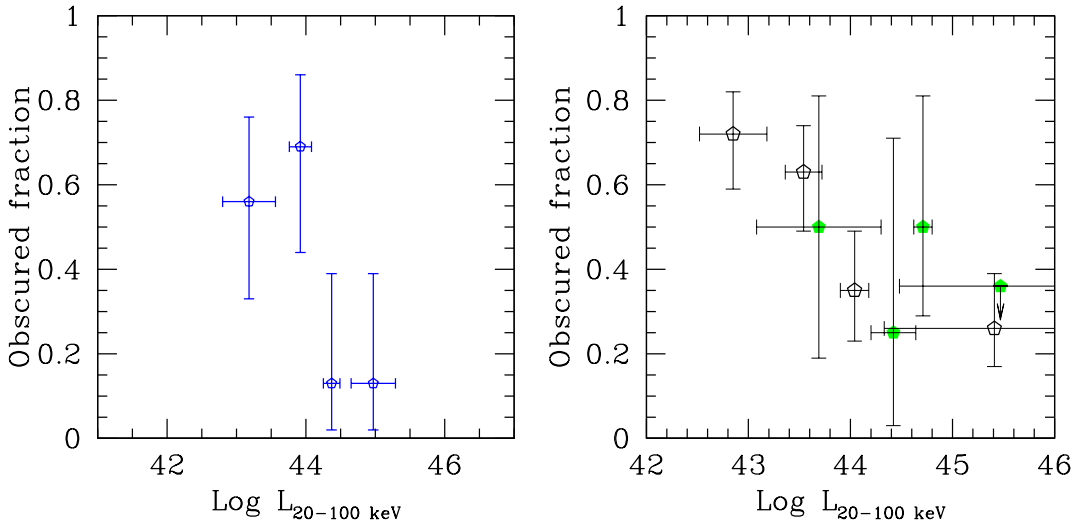

Figure 6. Fraction of obscured AGN (number of objects with $N_H > 10^{22}$ cm^{-2} over the total number) versus luminosity bins, computed for the 64 hard X-ray selected radio galaxies (left panel). Fraction of obscured AGN versus luminosity bins, computed for the Malizia et al. (2012) sample (right panel). Non-radio galaxies objects are drawn as black empty polygons, while radio galaxies as green solid polygons.

very small, generating very large error bars, nonetheless, the fraction of obscured radio galaxies seems to follow the same trend in luminosity as obscured non-radio galaxies. A dependence of obscured sources with redshift cannot be tested with our flux limited sample, as it would suffer from observational biases. However, a possible evolution of the CT radio galaxies population with redshift was suggested by the work from Wilkes et al. (2013), who have estimated a fraction of CT AGN of 21 ± 0.7 % in high redshift radio galaxies ($1 < z < 2$). A confirmation to this result must come from the study of large samples at different redshifts ranges.

5 CONCLUSIONS

We have presented for the first time the observed column density distribution of a sample of hard X-ray selected radio galaxies. The sample consists of 64 radio galaxies (mostly FRII), all within z<1, of relatively high luminosities (from 10^{42} to 10^{46} erg/s) and accreting at high Eddington ratios. All of them have an accurate measure of the column density and an accurate optical classification (except for two sources). Similarly to non-radio hard-X selected sources, we have found a fraction of $\sim$ 40% of absorbed sources among the total sample, and $\sim$ 75% among type 2 AGN. On the other hand the observed fraction of CT AGN is $\sim$ 2-3% compared to the 5-7% found in non-radio galaxies hard X-ray selected AGN (Malizia et al. 2009, Burlon et al. 2011). These results confirms that, at the zeroth order, unified models apply in a similar way to AGN with jets. This is also confirmed by a recent study from Gupta et al. (2016) in which the dust covering factors of FRII and Quasars show a very similar distribution, suggesting similar accretion conditions on parsec scales among the two classes.

Among radio galaxies, a handful of objects apparently deviate from the unified models predictions, i.e., the optical classification do not match with the X-ray classification. Six objects display broad emission lines in their optical spectra but their X-ray spectra are absorbed. However, the absorption usually comes from ionized material not associated with the classical torus, therefore the unified models predictions are not invalidated. One object is a type 2 AGN and has no X-ray absorption. Our simultaneous multi-frequency observations will allow to rule out variability as a possible cause for such mismatch.

Finally, we have estimated the absorption and CT fractions in a sample of non-radio galaxies and radio galaxies extracted from the same sample selected at hard X-ray (from Malizia et al. 2012) and therefore subject to the same biases effects. We find that the fraction of absorbed AGN is comparable among non-radio galaxies and radio galaxies (49^{+6}_{-7}% and 35^{+22}_{-17}%, respectively) while the fraction of CT AGN is only slightly larger in non-radio galaxies (6±3%) compared to radio galaxies (<1. 4%). We have selected one non-radio galaxies and one radio galaxies sub-sample in the same redshift range and then in the same flux range in order to exclude further biases, and overall we find that the fraction of absorbed AGN is always comparable (within errors) among the two groups, while there is a marginal evidence that the fraction of CT is always slightly smaller in radio galaxies. We have also checked for a possible dependence of the absorbed population on the luminosity as suggested in the literature. We found that the fraction of absorbed radio galaxies decreases with luminosity as well as non-radio galaxies. Unfortunately, the small number of sources tested here prevent us from drawing a firm conclusion. Ideally, statistically significant samples at different redshifts are needed to confirm such trend. INTEGRAL and *Swift* are continuing in their survey of the hard X-ray sky reaching sensitivity levels down to 10^{-12} ergs cm^{-2} s^{-1} allowing to detect new sources and to increase the sample of non-radio galaxies and radio galaxies (Bird et al. 2016, Mereminskiy et al. 2016, Malizia et al. 2016). In the future, SKA surveys will trace the low-power radio-loud AGN population at

a flux level of 1μJy (Prandoni & Seymour 2015) and in synergy with *Athena* it will be possible to investigate the evolution of the fraction of absorbed objects with X-ray luminosity and redshift up to z $\sim$ 4 - 5.

Acknowledgements

FP acknowledges support from INTEGRAL ASI/INAF n.2013-025-R.0. FP thanks Matteo Guainazzi and Paola Grandi for helpful discussions. The authors acknowledge the use of NED, SIMBAD and HEASARC.

REFERENCES

Abdo, A. A., Ackermann, M., Ajello, M., et al. 2010, ApJ, 720, 912
Ajello, M., Costamante, L., Sambruna, R. M., et al. 2009, ApJ, 699, 603
Ajello, M., Rau, A., Greiner, J., et al. 2008, ApJ, 673, 96-113
Akylas, A., & Georgantopoulos, I. 2009, A&A, 500, 999
Alexander, D. M., Bauer, F. E., Brandt, W. N., et al. 2011, ApJ, 738, 44
Alexander, D. M., Bauer, F. E., Chapman, S. C., et al. 2005, ApJ, 632, 736
Antonucci, R. 1993, ARA&A, 31, 473
Aird, J., Coil, A. L., Georgakakis, A., et al. 2015, MNRAS, 451, 1892
Aird J., et al., 2015, ApJ, 815, 66
Bassani, L., Dadina, M., Maiolino, R., et al. 1999, ApJS, 121, 473
Baumgartner, W. H., Tueller, J., Markwardt, C. B., et al. 2013, ApJS, 207, 19
Belsole, E., Worrall, D. M., & Hardcastle, M. J. 2006, MNRAS, 366, 339
Bettoni, D., Falomo, R., Fasano, G., & Govoni, F. 2003, A&A, 399, 869
Bianchi, S., Panessa, F., Barcons, X., et al. 2012, MNRAS, 426, 3225
Bird, A. J., Bazzano, A., Malizia, A., et al. 2016, ApJS, 223, 15
Bird, A. J., Bazzano, A., Bassani, L., et al. 2010, ApJS, 186, 1
Best, P. N., & Heckman, T. M. 2012, MNRAS, 421, 1569
Bondi, M., Gregorini, L., Padrielli, L., & Parma, P. 1993, A&AS, 101, 431
Brightman, M., & Nandra, K. 2011, MNRAS, 414, 3084
Buchner, J., Georgakakis, A., Nandra, K., et al. 2015, ApJ, 802, 89
Burlon, D., Ajello, M., Greiner, J., et al. 2011, ApJ, 728, 58
Buttiglione, S., Capetti, A., Celotti, A., et al. 2009, A&A, 495, 1033
Capetti, A., Fanti, R., & Parma, P. 1995, A&A, 300, 643
Cappi M., et al., 2006, A&A, 446, 459
Cao, X., & Rawlings, S. 2004, MNRAS, 349, 1419
Chiaberge, M., Capetti, A., & Celotti, A. 2002, A&A, 394, 791
Condon, J. J., Cotton, W. D., Greisen, E. W., et al. 1998, AJ, 115, 1693
Cusumano, G., La Parola, V., Romano, P., et al. 2010, MNRAS, 406, L16
de Bruyn, A. G. 1989, A&A, 226, L13
Drouart, G., De Breuck, C., Vernet, J., et al. 2012, A&A, 548, A45
Duncan, R. A., & Sproats, L. N. 1992, Proceedings of the Astronomical Society of Australia, 10, 16
Eguchi, S., Ueda, Y., Awaki, H., et al. 2011, ApJ, 729, 31
Eguchi, S., Ueda, Y., Terashima, Y., Mushotzky, R., & Tueller, J. 2009, ApJ, 696, 1657
Evans, D. A., Hardcastle, M. J., Lee, J. C., et al. 2008, ApJ, 688, 844-851
Evans, D. A., Worrall, D. M., Hardcastle, M. J., Kraft, R. P., & Birkinshaw, M. 2006, ApJ, 642, 96
Fan, J. H., & Zhang, J. S. 2003, A&A, 407, 899
Fanaroff, B. L., & Riley, J. M. 1974, MNRAS, 167, 31P
Fiore, F., Puccetti, S., Brusa, M., et al. 2009, ApJ, 693, 447
Fuerst, F., Mueller, C., Madsen, K. K., et al. 2015, arXiv:1511.01915
Gehrels, N. 1986, ApJ, 303, 336
Gendre, M. A., Best, P. N., Wall, J. V., & Ker, L. M. 2013, MNRAS, 430, 3086
Gilli R., Comastri A., Hasinger G., 2007, A&A, 463, 79
Grandi, P., Malaguti, G., & Fiocchi, M. 2006, ApJ, 642, 113
Greene, J. E., & Ho, L. C. 2007, ApJ, 670, 92
Guainazzi, M., Siemiginowska, A., Stanghellini, C., et al. 2006, A&A, 446, 87
Guainazzi, M., Siemiginowska, A., Rodriguez-Pascual, P., & Stanghellini, C. 2004, A&A, 421, 461
Gupta, M., Sikora, M., & Nalewajko, K. 2016, arXiv:1603.03670
Hardcastle, M. J., Evans, D. A., & Croston, J. H. 2009, MNRAS, 396, 1929
Hardcastle, M. J., Evans, D. A., & Croston, J. H. 2006, MNRAS, 370, 1893
Hasenkopf, C. A., Sambruna, R. M., & Eracleous, M. 2002, ApJ, 575, 127
Hine, R. G., & Longair, M. S. 1979, MNRAS, 188, 111
Iwasawa, K., Gilli, R., Vignali, C., et al. 2012, A&A, 546, A84
Jamrozy, M., Konar, C., Saikia, D. J., et al. 2007, MNRAS, 378, 581
Jarosik, N., Bennett, C. L., Dunkley, J., et al. 2011, ApJS, 192, 14
Jia, J., Ptak, A., Heckman, T., & Zakamska, N. L. 2013, ApJ, 777, 27
Jones, P. A., Lloyd, B. D., & McAdam, W. B. 2001, MNRAS, 325, 817
Kataoka, J., Stawarz, Ł., Takahashi, Y., et al. 2011, ApJ, 740, 29
Kim, M., Ho, L. C., Peng, C. Y., et al. 2008, ApJ, 687, 767
Krivonos, R., Tsygankov, S., Lutovinov, A., et al. 2012, A&A, 545, A27
Krivonos, R., Tsygankov, S., Revnivtsev, M., et al. 2010, A&A, 523, A61
Lacy, M., Storrie-Lombardi, L. J., Sajina, A., et al. 2004, ApJS, 154, 166
Landi, R., Bassani, L., Malizia, A., et al. 2010, MNRAS, 403, 945
La Franca F., et al., 2005, ApJ, 635, 864

Lansbury G. B., et al., 2015, ApJ, 809, 115
Lawrence, A. 1991, MNRAS, 252, 586
Lister, M. L., Gower, A. C., & Hutchings, J. B. 1994, AJ, 108, 821
Liu, Y., Jiang, D. R., & Gu, M. F. 2006, ApJ, 637, 669
Maiolino R., Rieke G. H., 1995, ApJ, 454, 95
Malizia, A., Landi, R., Molina, M., et al. 2016, arXiv:1604.06303
Malizia, A., Molina, M., Bassani, L., et al. 2014, ApJ, 782, L25
Malizia A., Bassani L., Bazzano A., Bird A. J., Masetti N., Panessa F., Stephen J. B., Ubertini P., 2012, MNRAS, 426, 1750
Malizia, A., Stephen, J. B., Bassani, L., et al. 2009, MNRAS, 399, 944
Malizia, A., Landi, R., Bassani, L., et al. 2007, ApJ, 668, 81
Marchesini, D., Celotti, A., & Ferrarese, L. 2004, MNRAS, 351, 733
Masetti, N., Parisi, P., Palazzi, E., et al. 2013, A&A, 556, A120
Matt, G., Bianchi, S., Guainazzi, M., Barcons, X., & Panessa, F. 2012, A&A, 540, A111
Mauch, T., Murphy, T., Buttery, H. J., et al. 2003, MNRAS, 342, 1117
McLure, R. J., Jarvis, M. J., Targett, T. A., Dunlop, J. S., & Best, P. N. 2006, MNRAS, 368, 1395
Mereminskiy, I. A., Krivonos, R. A., Lutovinov, A. A., et al. 2016, arXiv:1602.00463
Mezcua, M., Lobanov, A. P., Chavushyan, V. H., & León-Tavares, J. 2011, A&A, 527, A38
Miller, B. P., & Brandt, W. N. 2009, ApJ, 695, 755
Mingo, B., Hardcastle, M. J., Croston, J. H., et al. 2014, MNRAS, 440, 269
Molina, M., Giroletti, M., Malizia, A., et al. 2007, MNRAS, 382, 937
Molina, M., Landi, R., Bassani, L., et al. 2012, A&A, 548, A32
Molina, M., Bassani, L., Malizia, A., et al. 2014, A&A, 565, A2
Molina, M., Venturi, T., Malizia, A., et al. 2015, MNRAS, 451, 2370
Morganti, R., Killeen, N. E. B., & Tadhunter, C. N. 1993, MNRAS, 263, 1023
Morganti, R., Oosterloo, T., Tadhunter, C. N., et al. 1999, A&AS, 140, 355
Panessa F., Bassani L., Cappi M., Dadina M., Barcons X., Carrera F. J., Ho L. C., Iwasawa K., 2006, A&A, 455, 173
Page, K. L., Schartel, N., Turner, M. J. L., & O'Brien, P. T. 2004, MNRAS, 352, 523
Panessa, F., & Bassani, L. 2002, A&A, 394, 435
Prandoni, I., & Seymour, N. 2015, Advancing Astrophysics with the Square Kilometre Array (AASKA14), 67
Osterbrock, D. E. 1981, ApJ, 249, 462
Owen, F. N., & Laing, R. A. 1989, MNRAS, 238, 357
Reid, R. I., Kronberg, P. P., & Perley, R. A. 1999, ApJS, 124, 285
Reynolds, C. S., Lohfink, A. M., Ogle, P. M., et al. 2015, ApJ, 808, 154
Risaliti, G., Maiolino, R., & Salvati, M. 1999, ApJ, 522, 157
Rottgering, H. J. A., Tang, Y., Bremer, M. A. R., et al. 1996, MNRAS, 282, 1033
Runnoe, J. C., Brotherton, M. S., Shang, Z., & DiPompeo, M. A. 2013, MNRAS, 434, 848
Sambruna, R. M., Reeves, J. N., & Braito, V. 2007, ApJ, 665, 1030
Sambruna, R. M., Eracleous, M., & Mushotzky, R. F. 1999, ApJ, 526, 60
Sazonov, S., Churazov, E., & Krivonos, R. 2015, MNRAS, 454, 1202
Sazonov, S., Revnivtsev, M., Krivonos, R., Churazov, E., & Sunyaev, R. 2007, A&A, 462, 57
Sbarrato, T., Ghisellini, G., Maraschi, L., & Colpi, M. 2012, MNRAS, 421, 1764
Schoenmakers, A. P., Mack, K.-H., Lara, L., et al. 1998, A&A, 336, 455
Siemiginowska, A., LaMassa, S., Aldcroft, T. L., Bechtold, J., & Elvis, M. 2008, ApJ, 684, 811-821
Slee, O. B., Sadler, E. M., Reynolds, J. E., & Ekers, R. D. 1994, MNRAS, 269, 928
Sobolewska, M. A., Siemiginowska, A., Migliori, G., et al. 2012, ApJ, 758, 90
Sadoun, R., & Colin, J. 2012, MNRAS, 426, L51
Sazonov S., Churazov E., Krivonos R., 2015, MNRAS, 454, 1202
Tadhunter, C., Marconi, A., Axon, D., et al. 2003, MNRAS, 342, 861
Tazaki, F., Ueda, Y., Terashima, Y., Mushotzky, R. F., & Tombesi, F. 2013, ApJ, 772, 38
Tazaki, F., Ueda, Y., Ishino, Y., et al. 2010, ApJ, 721, 1340
Tombesi, F., Tazaki, F., Mushotzky, R. F., et al. 2014, MNRAS, 443, 2154
Torresi, E., Grandi, P., Costantini, E., & Palumbo, G. G. C. 2012, MNRAS, 419, 321
Torresi, E., Grandi, P., Guainazzi, M., et al. 2009, A&A, 498, 61
Treister, E., & Urry, C. M. 2006, ApJ, 652, L79
Trippe, M. L., Crenshaw, D. M., Deo, R. P., et al. 2010, ApJ, 725, 1749
Urry, C. M., & Padovani, P. 1995, PASP, 107, 803
Ueda, Y., Akiyama, M., Hasinger, G., Miyaji, T., & Watson, M. G. 2014, ApJ, 786, 104
Ueda, Y., Eguchi, S., Terashima, Y., et al. 2007, ApJ, 664, L79
Ueda, Y., Akiyama, M., Ohta, K., & Miyaji, T. 2003, ApJ, 598, 886
van der Wolk, G., Barthel, P. D., Peletier, R. F., & Pel, J. W. 2010, A&A, 511, A64
Vasudevan, R. V., Mushotzky, R. F., & Gandhi, P. 2013, ApJ, 770, L37
Vasudevan, R. V., & Fabian, A. C. 2007, MNRAS, 381, 1235
Vignali, C., Mignoli, M., Gilli, R., et al. 2014, A&A, 571, A34
Wandel, A. 2002, ApJ, 565, 762
Wang, J., Mao, Y. F., & Wei, J. Y. 2009, AJ, 137, 3388
Wilkes, B. J., Kuraszkiewicz, J., Haas, M., et al. 2013, ApJ, 773, 15
Wilman, R. J., Edge, A. C., & Johnstone, R. M. 2005, MNRAS, 359, 755
Winter, L. M., Lewis, K. T., Koss, M., et al. 2010, ApJ, 710, 503
Winter, L. M., Mushotzky, R. F., Tueller, J., & Markwardt,

C. 2008, ApJ, 674, 686
Woo, J.-H., & Urry, C. M. 2002, ApJ, 579, 530
Wu, X.-B., & Liu, F. K. 2004, ApJ, 614, 91
Wu, Q. 2009, MNRAS, 398, 1905

Table 1. Radio Galaxies detected by *INTEGRAL*/IBIS and *Swift*/BAT

Name	**z**	**Opt Class**	**Radio Morph**	**Log $N_{\mathbf{H}}$**	**F(2–10 keV)**†	**F_{BAT}**† (20–100 keV)	**F_{IBIS}**† (20–100 keV)	**Ref.**	Log M_{BH}	**Ref.**	R_{core}	**Ref.**
PKS 0018–19	0.095579	Sy1.9	FR II	21.89 [21.83 – 21.95]	1.07	1.19	–	1	–	–	0.186	1
PKS 0101–649	0.163000	BLQSO	FR II	**20.36**	0.31	0.63	–	1	–	–	–	–
3C 033	0.059700	Sy2	FR II	23.72 [23.69 – 23.80]	0.27	1.71	–	2	8.48	1	0.003	2
NGC 612	0.029771	Sy2	FR I/II	24.04 [24.02 – 24.06]	1.60	3.04	–	3	8.64	1	0.009	3
3C 059	0.109720	Sy1.8	FR II	**20.78**	0.84	1.07	–	4	7.15	2	0.034	4
3C 062	0.147000	Sy2	FR II	23.26 [23.18 – 23.36]	0.2	0.77	–	5	8.81	1	0.005	1
4C +10.08	0.070000	NLRG	FR II	21.89[21.69 – 22.05]	0.23	0.87	–	1	–	–	–	–
QSO B0309+411B	0.134000	Sy1	FR II	**21.11**	2.36	0.96	1.90	6	–	–	3.0	5
2MASX J03181899+6829322	0.090100	Sy1.9	FR II	22.61 [22.57 – 22.66]	0.73	1.03	1.34	6	–	–	0.133	6
NGC 1275	0.017559	Sy1.5	FR I	21.08 [21.04 – 21.11]	1.23	3.80	3.00	6	8.5	3	0.646	7
3C 098	0.0304	Sy2	FR II	23.08 [23.00 – 23.18]	0.27	–	3.80	6	7.88	4	0.0017±0.0005	8
3C 105	0.089000	Sy2	FR II	23.45 [23.40 – 23.47]	0.21	1.69	3.10	6	8.61	5	0.006	3
3C 109	0.305600	Sy1.8	FR II	21.70 [21.60 – 21.78]	0.80	0.82	–	7	8.30	6	0.06±0.02	8
3C 111	0.048500	Sy1	FR II	21.66 [21.63 – 21.69]	3.51	7.13	10.50	6	8.80	7	0.04±0.02	8
3C 120	0.033010	Sy1	FR I?	21.10 [21.19 – 21.22]	4.60	5.73	7.58	6	7.75	7	0.67	3
PKS 0442–28	0.147000	Sy2	FR II	21.93 [21.73 – 22.07]	1.16	1.14	–	5	9.11	5	0.041	9
Pic A	0.035058	Liner/Sy1	FR II	**20.78**	1.13	2.36	3.24	6	8.70	7	0.07	3
PKS 0521–364	0.056546	Sy1	FR I/II	**20.55**	1.10	2.00	2.19	6	8.6	8	0.176	3
PKS 0707–35	0.110800	Sy2	FR II	22.71[22.38 – 22.72]	0.56	1.19	–	8	–	–	–	–
3C 184.1	0.118200	Sy2	FR II	23.03[22.88 – 23.16]	0.26	0.69	–	9	8.32	9	–	–
B3 0749+460A	0.051799	Sy1.9	FR II	**20.25**	0.30	0.84	–	1	6.9	10	–	–
3C 206	0.197870	Sy1.2	FR II	**20.75**	1.50	1.52	–	8	8.86	11	0.273	1
4C +29.30	0.064715	Sy2	FR I/II	23.70 [23.68 – 23.71]	0.11	0.95	–	10	8.2	12	0.429±0.134	8
3C 227	0.086272	Sy1.5	FR II	22.16 [22.10 – 22.22]	2.36	1.52	–	5	8.90	7	0.0123	3
VII Zw 292	0.058100	Sy2	FR II	23.96 [23.80 – 24.16]	0.08	0.94	–	11	–	–	0.006	10
3C 234	0.184925	Sy1.9	FR II	23.81 [23.79 – 23.83]	0.13	0.48	–	12	8.99	13	0.02±0.006	8
PKS 1143–696	0.244000	Sey1.2	FR II	**21.21**	0.54	0.92	1.28	6	8.62	14	–	–
IGRJ13107–5626	-	-	FR II?	23.59 [23.41 – 23.80]	0.11	1.02	0.87	13	–	–	–	–
CenA	0.00088	Sey2	FR I	23.17 [23.16 – 23.18]	21.20	82.73	59.00	6	9.11	15	0.125	3
CenB	0.012916	NLRG	FR I/II	21.11 [21.98 – 22.21]	0.49	–	1.77	6	–	–	0.07±0.02	8
3C 287.1	0.2156	Sy 1	FR II	**21.21**	0.28	–	1.50	6	8.49	16	0.365±0.114	8
2MASX J14364961–1613410	0.144537	BLQSO	FR I/II	**20.88**	0.72	1.08	–	1	8.64	17	–	–
IGR 14488–4008	0.123	Sey1.2	FR II	22.89 [22.74 – 23.04]	0.53	0.82	0.60	14	8.58	14	–	–
3C 309.1	0.905000	Sy1.5	C	< 20.50	0.17	0.54	–	15	9.1	18	1.87±0.58	8
4C +63.22	0.20400	Sy1	FR II	**20.17**	0.36	0.56	–	1	–	–	0.028	10
3C 323.1	0.264300	Sy1.2	FR II	20.78 [20.00 – 21.04]	0.55	0.64	–	16	9.12	19	0.046±0.014	8
4C +23.42	0.118000	Sy1	FR I	21.75 [21.60 – 21.86]	0.32	0.79	–	1	–	–	–	–
Leda 100168	0.183000	Sy1	FR II	< 20.69	0.43	0.74	–	1	–	–	–	–
3C 332	0.151019	Sy1	FR II	**20.30**	0.58	1.34	–	4	8.64	16	–	–
Mrk 1498	0.054700	Sy1.9	FR II	23.76 [23.67 – 23.84]	0.90	2.69	–	17	8.59	20	0.09	11
4C +34.47	0.206000	Sy1	FR II	**20.49**	0.94	1.24	–	18	8.01	11	0.86±0.26	8
PKS 1737–60	0.410000 Phot	-	FR II	**20.77**	0.73	0.84	–	1	–	–	–	–
4C +18.51	0.186000	Sy1	FR II	**20.74**	0.49	0.59	–	1	9.35	21	0.1	12
IGR J17488–2338	0.240	Sy1.5	FR II	22.06 [21.96 – 22.15]	0.20	–	1.40	19	9.11	14	0.179	13

Name	**z**	**Opt Class**	**Radio Morph**	**Log $N_{\mathbf{H}}$**	**F(2–10 keV)**†	**F_{BAT}**† (20–100 keV)	**F_{IBIS}**† (20–100 keV)	**Ref.**	Log M_{BH}	**Ref.**	R_{core}	**Ref.**
3C 380	0.692000	Sy1.5	FR II	**20.75**	0.40	0.96	–	20	9.4	18	0.817±0.254	8
3C 382	0.057870	Sy1	FR II	**20.79**	5.98	5.32	4.24	6	8.90	21	0.05±0.02	8
3C 390.3	0.056100	Sy1.5	FR II	**20.63**	2.14	6.20	5.90	6	8.80	21	0.09±0.03	8
PKS 1916–300	0.166819	Sy1.5/1.8	FR II	**20.90**	0.62	0.97	0.99	6	–	–	0.02	14
3C 403	0.059000	Sy2	FR II	23.65 [23.58 – 23.62]	1.30	1.96	1.87	6	8.96	5	0.004	3
Cygnus A	0.056075	Sy1.9	FR II	23.30 [23.25 – 23.32]	1.20	8.29	8.49	6	9.40	22	0.002	3
PKS 2014–55	0.060629	Sy2	FR I	23.51 [23.36 – 23.64]	0.39	1.94	–	1	–	–	–	–
4C +21.55	0.173500	Sy1	FR II	21.78 [21.62 – 22.09]	1.40	1.98	2.91	21	–	–	–	–
4C +74.26	0.104000	Sy1	FR II	21.15 [21.04 – 21.20]	2.53	3.18	4.16	6	9.37	7	0.95±0.29	8
S5 2116+81	0.084000	Sy1	FR I	**21.38**	1.21	2.14	3.04	6	8.12	7	1.80±0.54	8
4C 50.55	0.020000	Sy1	FR II	22.89 [22.79 – 22.99]	4.88	12.25	12.50	6	7.80	23	0.1	15
3C 433	0.101600	Sy2	FR I/FR II	22.94 [22.90 – 23.97]	0.10	1.02	–	22	9.10	24	0.0011±0.0003	8
PKS 2135–14	0.20047	Sy1.5	FR II	23.26 [23.02 – 23.48]	0.57	0.90	–	5	9.65	5	0.096	3
PKS 2153–69	0.028273	Sy1	FR II	**20.40**	0.72	0.84	–	9	–	–	0.03±0.01	8
2MASX J22194971+2613277	0.085000	Sy1	FR II	21.40 [21.30 – 21.49]	0.67	1.03	–	1	–	–	–	–
3C 445	0.055879	Sy1.5	FR II	23.35 [23.26 – 23.46]	0.67	2.63	–	23	8.89	5	0.04	3
3C 452	0.081100	Sy2	FR II	23.77 [23.70 – 23.83]	0.50	1.97	2.75	6	8.54	13	0.06±0.018	8
PKS 2300–18	0.128929	Sy1	FR II?	**20.34**	0.51	0.70	–	1	8.25	25	1.07	1
PKS 2331–240	0.047700	Sy2	FR II	**20.21**	0.71	0.85	–	1	–	–	0.65	16
PKS 2356-61	0.096306	Sy2	FR II	23.17 [23.13 – 23.21]	0.20	0.91	–	5	8.96	5	0.008	3

† The 2–10 and 20–100 keV fluxes are in unit of 10^{-11} erg cm^{-2} s^{-1}. X-ray references: 1. This work; 2. Torresi et al. (2009); 3. Eguchi et al. (2011); 4. Tombesi et al. (2014); 5. Mingo et al. (2014); 6. Malizia et al. (2012); 7. Hardcastle et al (2006); 8. Tazaki et al. (2013); 9. Grandi et al. (2006); 10. Sobolewska et al. (2012); 11. Evans et al. (2008); 12. Vasudevan et al. (2013); 13. Landi et al. (2010); 14. Molina et al. (2015); 15. Siemiginowska et al. (2008); 16. Hasenkopf et al. (2002); 17. Eguchi et al. (2009); 18. Page et al. (2004); 19. Molina et al. (2014); 20. Belsole et al. (2006); 21. Malizia et al. (2016); 22. Miller & Brandt (2009); 23. Sambruna et al. (2007). Black hole mass references: 1. Bettoni et al. (2003); 2.Wandel (2002); 3.Wilman et al.(2005); 4. Woo & Urry (2002); 5. Mingo et al.(2014); 6. McLure et al. (2006); 7. Kataoka et al. (2011); 8. Sbarrato et al.(2012); 9. Grandi et al. (2006); 10. Greene & Ho (2007); 11. Liu et al. (2006); 12. Sobolewska et al. (2012); 13. Marchesini et al. (2004); 14. Masetti et al.(2013); 15. Sadoun & Coulin (2012); 16. Mezcua et al. (2011); 17. Kim et al. (2008); 18. Wu (2009); 19. Runnoe et al. (2013); 20. Winter et al. (2010); 21. Wang, Mao & Wei (2009); 22. Tadhunter et al. (2003); 23. Tazaki et al. (2010); 24. Cao & Rawlings (2004); 25. Wu & Liu (2004). 5 GHz radio core dominance references: 1. Reid et al. (1999); 2. Hardcastle et al. (1998); 3. Morganti et al. (1993); 4. Bondi et al. (1993); 5. De Bruyn et al. (1989); 6. Schoenmakers et al. (1998); 7. Abdo et al. (2010); 8. Fan & Zhang (2003); 9. Morganti et al. (1999); 10. Lara et al. (2001), at 1.4 GHz; 11. Rottgering et al. (1996); 12. Lister, Gower & Hutchings (1994); 13. Molina et al. (2014); 14. Duncan & Sprooats (1992); 15. Molina et al. (2007); 16. Slee et al (1994).

APPENDIX A: *SWIFT*/XRT DATA REDUCTION AND ANALYSIS

We took all radio galaxies from the sample of Bassani et al. (2016) and extracted 13 objects for which X-ray spectral information were not found in the literature. This list of sources was then cross-correlated with the *Swift*/XRT archival dataset, and for all sources we found X-ray observations available in the archive. The log of all X-ray observations analysed in this work is given in Table A1, where we report for each individual radio galaxy, the XRT observation ID, the date and the exposure of the XRT pointings.

The XRT data were processed using the XRTDAS standard data pipeline package (XRTPIPELINE v. 0.12.9) to produce calibrated and cleaned PC-mode event file. Observations were summed together using XSELECT V. 2.4C. XRT images in the 0.3–10 keV energy band were obtained and analysed by means of the software package XIMAGE v. 4.5.1. We found that all sources were detected by XRT, although not all with good statistical significance.

For the spectral analysis, source events were extracted within a circular region with a radius of 20 pixels (1 pixel $\sim$ 2.36 arcsec) centred on the source position, while background events were extracted from a source-free region close to the X-ray source of interest. The spectra were obtained from the corresponding event files using the XSELECT V. 2.4C software and binned using GRPPHA in an appropriate way, so that the χ^2 statistic could be applied. We used version v.014 of the response matrices and created individual ancillary response files *arf* using XRTMKARF V. 0.6.0.

Next, we combined the XRT spectra with the BAT ones (from the 70-month BAT catalogue, Baumgartner et al. 2013)[5] to perform the spectral analysis over the 0.3–100 keV energy range. We adopted a simple absorbed power law model to fit the source spectra where absorption is partly due to a Galactic column density in the source direction (fixed value) and partly to an intrinsic column density (free parameter). We also introduced in the fitting procedure a cross-calibration constant (C_{calib}) to account for a possible mismatch between XRT and BAT data, as well as for source flux variations.

The results of the spectral fittings are shown in Table A2 where we report for each source the value of the Galactic column density, the photon index, the 2–10 keV Luminosity, the χ^2/ν values of the fit, and the XRT/BAT cross-correlation constant, while intrinsic absorption values, as well as 2–10 keV fluxes are given in Table 1 of the main text. In the fitting procedure, when no absorption is measured, the Galactic column density value is used as an upper limit to the amount of absorption.

Those sources for which this simple model does not fit the data properly, indicating the need for an extra feature, are briefly discussed in the following sections.

4C +63.22

For this source, our baseline model does not provide a good fit to the data ($\chi^2/\nu = 69.0/43$) as residuals, indicative of an absorbing feature at around 0.9 keV, are clearly visible in the data-to-model ratio. We therefore tested our data for the presence of an absorption edge, leaving all the parameters free to vary: the fit improves significantly ($\chi^2/\nu = 38.4/41$) and the component is required by the data at more than 99.99% confidence level (c.l.). The absorption edge turned out to be at 0.94 ± 0.06 and have $\tau_{max} = 0.91^{+0.34}_{-0.30}$, thus indicating an origin from Fe XX. This result is not surprising as Molina et al. (2015) have recently detected absorption features from ionised elements in the giant radio galaxy IGR J14488–4008.

PKS 2014−55

This is another case in which the baseline model do not provide a good fit to the data ($\chi^2/\nu = 35.8/12$) as an excess below 1 keV is observed in the residuals. Also in this case we added to the baseline model a second power law passing through intrinsic absorption, having the same photon index of the primary one, which yields an improvement ($> 99.99\%$) of the fit as shown in Table A2

PKS 2300−18

For this source, there is a hint of an excess around 6 keV, again due to neutral iron, which we modelled by adding a narrow line component. This feature is required at around 99.8% ($\Delta\chi^2/\nu = 14.6/2$) and provides a line centroid at 6.51 ± 0.10 and an $EW = 608^{+267}_{-272}$ eV.

[5] available at: http://swift.gsfc.nasa.gov/results/bs70mon/.

Table A1. Log of the *Swift*/XRT observations used in this paper.

Source name	ID	Obs date	Exposure (s)
PKS 0018−19	00040886001	Sep 27, 2010	8037
	00040691001	Jan 30, 2011	6494
total obs	–	–	14531
PKS 0101−649	00047109001	Nov 01, 2011	864
	00047109002	Nov 11, 2011	2778
	00047109003	Nov 17, 2011	166
	00047109004	Nov 20, 2011	241
	00047109005	Nov 23, 2011	637
	00047109006	Nov 25, 2011	2641
	00047109007	Apr 05, 2012	2101
total obs	–	–	9428
4C +10.08	00037347001	Dec 05, 2010	527
	00037347002	Dec 14, 2010	6956
	00037347003	Mar 02, 2011	1143
	00037347004	Mar 06, 2011	2061
total obs			10687
B3 0749+460A	00037357001	Feb 24, 2008	9353
2MASX J14364961−1613410	00040978001	Dec 25, 2010	595
	00040978002	Apr 12, 2011	222
	00047122001	Apr 12, 2012	193
	00047122003	May 08, 2013	632
	00047122004	May 10, 2013	110
	00047122005	May 20, 2013	865
	00047122006	May 21, 2013	2775
	00047122007	May 26, 2013	341
	00047122008	May 27, 2013	3874
total obs			9607
4C +63.22	00035401002	Oct 17, 2006	5546
4C +23.42	00038073001	Sep 25, 2008	2269
	00038073002	Sep 26, 2008	4930
	00038073004	Jan 04, 2009	6690
total obs			13889
LEDA 100168	00037998001	Jul 05, 2008	4885
	00037998002	Jul 06, 2008	2563
	00037998002	Jul 06, 2008	2563
	00037998002	Jul 07, 2008	2532
total obs			9980
PKS 1737−60	00047123001	Nov 10, 2011	836
	00047123002	Nov 11, 2011	5204
	00047123003	Nov 14, 2011	1123
	00047123004	Nov 17, 2011	2871
total obs			10034
4C +18.51	00041782001	Oct 31, 2010	2490
	00041782002	Jan 13, 2011	1586
	00041782003	Jan 21, 2011	1715
	00041782004	Jan 25, 2011	1680
	00041782004	Jan 28, 2011	3003
total obs			10474
2MASX J22194971+2613277	00041122002	Jul 12, 2010	3181
	00041122003	Jul 13, 2010	7165
	00041122004	Jul 15, 2010	946
	00041122005	Jul 17, 2010	1991
total obs			13283
PKS 2331−240	00031731001	Jun 05, 2010	1668
	00031731002	Jun 05, 2010	3924
	00041128001	Sep 29, 2010	9052
total obs			14644

Table A2. XRT spectral analysis results.

Source name	$N^{a}_{H(Gal)}$	Γ	L(2–10 keV)^{b}	χ^2/ν	C^{c}_{calib}	Model
PKS 0018−19	0.0201	1.72 ± 0.12	2.37	105.5/109	$0.55^{+0.22}_{-0.16}$	absorbed pl
PKS 0101−649	0.0231	1.69 ± 0.09	2.16	33.8/48	$1.00^{+0.47}_{-0.34}$	simple pl
4C +10.08	0.100	$1.70^{+0.31}_{-0.29}$	0.262	17.7/21	$1.78^{+2.00}_{-0.99}$	absorbed pl
B3 0749+460A	0.0179	1.64 ± 0.08	0.188	61.9/49	$1.22^{+0.48}_{-0.36}$	simple pl
2MASX J14364961−1613410	0.0759	1.72 ± 0.06	3.90	74.5/93	$0.79^{+0.29}_{-0.23}$	simple pl
4C +63.22	0.0148	1.96 ± 0.08	4.30	38.4/41	$1.38^{+0.63}_{-0.46}$	simple pl + absorption edge
4C +23.42	0.0416	1.67 ± 0.21	1.11	46.3/38	$1.07^{+0.91}_{-0.50}$	absorbed pl
LEDA 100168	0.0593	1.75 ± 0.11	3.91	67.4/65	$0.97^{+0.45}_{-0.31}$	absorbed pl
PKS 1737−60	0.0584	1.94 ± 0.07	23.3	86.1/75	$1.55^{+0.72}_{-0.56}$	simple pl
4C +18.51	0.0551	1.83 ± 0.07	4.72	66.3/75	$0.81^{+0.41}_{-0.33}$	simple pl
PKS 2014−55	0.0481	1.86 ± 0.21	0.304	17.2/10	$1.01^{+0.72}_{-0.42}$	double pl
2MASX J22194971+2613277	0.0664	1.69 ± 0.11	1.18	70.1/85	$0.73^{+0.31}_{-0.22}$	abserbed pl
PKS 2300−18	0.0217	1.83 ± 0.21	2.24	139.0/117	$1.01^{+0.39}_{-0.33}$	simple pl + iron line
PKS 2331−240	0.0163	1.70 ± 0.04	0.375	147.5/138	$0.60^{+0.18}_{-0.16}$	simple pl

[a] In units of 10^{22} cm^{-2} (from Kalberla et al. 2005);

[c] IBIS/XRT cross-calibration constant;

[b] In units of 10^{44} erg s^{-1}.